This is a “preproof” accepted article for *Mineralogical Magazine*.

This version may be subject to change during the production process.

10.1180/mgm.2024.90

Parisite-(Nd), ideally $CaNd_2(CO_3)_3F_2$, a new mineral from Bayan Obo Fe-Nb-REE deposit, Inner Mongolia, China

CHENZI FAN[1,*], HONG YU[2], XIANGPING GU[3], PUSHENG ZENG[1] AND ZHENYU CHEN[2]

[1]National Research Centre for Geoanalysis, Baiwanzhuang Street 26, Beijing, 100037, China

[2]Institute of Mineral Resources, Chinese Academy of Geological Sciences, Baiwanzhuang Street 26, Beijing, 100037, China

[3]School of Geosciences and Info-Physics, Central South University, Changsha, Hunan 410083, China

Abstract

Parisite-(Nd) (IMA2024-013), ideally $CaNd_2(CO_3)_3F_2$, as the Nd-dominat analogue of parisite-(Ce), occurs in dolomitic marble in the Bayan Obo Fe-Nb-REE deposit, Inner Mongolia, China. It is associated with calcite, aegirine, magnetite, hematite, fluorite, riebeckite, bastnäsite-(Ce), barite, aeschynite-(Ce), aeschynite-(Nd), monazite, and parisite-(Ce). Parisite-(Nd) occurs as subhedral to anhedral irregular grains from 0.02 mm to 1 mm. Parisite-(Nd) is transparent, yellowish-brown color, with pale yellow streak and displays vitreous to resinous lustre. Cleavage is distinct on pseudo-{001}; fracture is uneven, or conchoidal. The Mohs hardness is 4 to 5, and it is brittle. Calculated density of parisite-(Nd) is 4.357 g/cm^3. Parisite-(Nd) is pseudo-uniaxial (+), ω= (1.679), ε = (1.754). The empirical formula is $(Ca_{0.945}Fe_{0.058}Sr_{0.015}Ba_{0.007})_{\Sigma 1.025}(Nd_{0.967}Ce_{0.529}La_{0.191}Pr_{0.137}Gd_{0.070}Sm_{0.029}Th_{0.022}Y_{0.016}Nb_{0.011}Ho_{0.003})_{\Sigma 1.975}(CO_3)_3F_{1.893}OH_{0.023}$. The Raman spectrums of parisite-(Nd) are observed strong and sharp peaks at 1113, 1090, 825, 635 and 1608 cm^{-1} and moderate to weak bands centered at 255, 392, 739, 924, 1183, 1228, 1296, 1640, 2247, 2924 and 3065 cm^{-1}. X-ray powder diffraction and TEM

* E-mail:czfan2013@163.com

studies give the following results: monoclinic, space group: *Cc* (# 9), *a* = 12.3283(13) Å, *b* = 7.1185(4) Å, *c*=28.4633(37) Å, β = 98.529(14)°, *V* = 2470.28(42) Å^3, Z = 12.

Keywords: parisite-(Nd), new mineral, Ca-REE fluorocarbonate, Bayan Obo deposit, Inner Mongolia, China

Introduction

Parisite-(Nd) is a new member mineral in calcium-rare earth element (Ca-REE) flurocarbonates. So far, four mineral species have been discovered in the Ca-REE flurocarbonate mineral series (Donnay and Donnay, 1953). Bastnäsite, $REECO_3F$ and synchysite, $CaREE(CO_3)_2F$ are considered as the end members of this polysomatic mineral series. Parisite, $CaREE_2(CO_3)_3F_2$, and röntgenite, $CaREE_2(CO_3)_3F_2$ are considered as intermediate members (Ni *et al*., 1993; Wu *et al*., 1998; Zeug *et al*., 2021). Rare earth elements are easy to replace each other in mineral crystal structures because of their similar properties. Cerium is the most common rare element in Ca-REE flurocarbonates. All the Ce-dominant analogues including bastnäsite-(Ce), röntgenite-(Ce), synchysite-(Ce) and parisite-(Ce) have been found in nature. The La-dominant analogues of bastnäsite-(La) and parisite-(La), Nd-dominant analogues of bastnäsite-(Nd) and synchysite-(Nd), Y-dominant analogues of bastnäsite-(Y) and synchysite-(Y) are also reported (Smith *et al*., 1960; Vainshtein *et al*., 1961; Mineev *et al*., 1970; Scharm and Kühn, 1983; Miyawaki *et al*., 2013; Menezes Filho *et al*., 2018). Parisite-(Nd) is the Nd-dominant analogue of parisite-(Ce) and parisite-(La).

Parisite-(Ce) has generated considerable interest because of its economic importance as the primary source rare earth elements for industrial use (Morteani, 1991). Parisite-(Ce), as one of the most common rare earth minerals, was first reported by J.J. Paris in 1835 from the emerald mine at Muzo in Colombia, South America (Warren and Palache, 1911). It occurs as an accessory mineral in differentiated alkalic massifs, granite pegmatites, and REE-rich carbonatites. It distributes in many localities, for example the carbonatite orebody of Mountain Pass, California (Castor, 2008), the carbonatite complex Amba Dongar, India (Doroshkevich *et al*., 2009), the alkaline granite-syenite pegmatites of the Mount Malosa pluton in Malawi (Guastoni *et al*., 2010),

https://doi.org/10.1180/mgm.2024.90 Published online by Cambridge University Press

the ultramafic lamprophyre–carbonatite complex near Delitzsch, Germany (Seifert *et al*., 2000), the Bayan Obo Fe–Nb–RE deposit, Inner Mongolia, China (Zhang and Tao, 1986). It has been reported with a chemical composition of $Ca_{1.02}(Ce_{0.94}La_{0.50}Nd_{0.37}Pr_{0.10}Sm_{0.05})_{\Sigma=1.96}(CO_3)_3F_{1.51}$ from Muso mine Colombia (NMNH no. 122145)(Ni *et al*., 2000). The crystal structure of parisite-(Ce) was once controversial. In an earlier study, its structure was defined as hexagonal symmetry with space group *R*3, a=7.18 Å, c=8.41 Å (Donnay and Donnay, 1953). Until the work of Ni *et al* (2000), the crystal structure of parisite-(Ce) was refined to monoclinic symmetry with space group *C*2/*c* or *Cc* and unit cell of a = 12.305(2), b = 7.1053(5), c = 28.250(5) Å, and β = 98.257(14)°. Parisite-(La) only discovered in the Mula mine, Brazil has been approved as a new mineral (IMA2016-031) with chemical composition of $Ca_{0.98}(La_{0.83}Nd_{0.51}Ce_{0.37}Pr_{0.16}Sm_{0.04}Y_{0.03})_{\Sigma1.94}C_{3.03}O_{8.91}F_{2.09}$ and crystal structure of monoclinic (pseudo-trigonal), space group: *C2*, *Cm*, or *C2/m*, a = 12.356(1) Å, b = 7.1368(7) Å, c = 28.299(3) Å, β =98.342(4)°, V = 2469.1(4) $Å^3$ and Z = 12 (Menezes Filho *et al*., 2018). Parisite-(Nd) was once reported in Bayan Obo deposit in the literature, but only REE assemblage information was provided, and no complete chemical compositions and crystal structure were given (Zhang and Tao, 1986). So it is not officially recognized by IMA CNMNC list (Jambor *et al*., 1988).

Now parisite-(Nd) has been approved as a new mineral species by the Commission of New Minerals, Nomenclature and Classification (CNMNC) of the International Mineralogical Association (IMA 2024-013) (Bosi *et al*., 2024). Type material is deposited in the collections of the National Research Center for Geoanalysis, Baiwanzhuang Street 26, Beijing, People's Republic of China (holotype), catalogue Number NRCGA2024001, and the Geological Museum of China, Yangrouhutong Street 15, Xicheng District, Beijing, People's Republic of China, catalogue number GMCTM2024003 (cotype).

Occurrence

Parisite-(Nd) was found in dolomitic marble in the Bayan Obo Fe-Nb-REE deposit, 130 km north of the city of Baotou, Inner Mongolia, China. Bayan Obo deposit is hosted by Palaeo- to Mesoproterozoic sedimentary rocks of the Bayan Obo Group (Nie *et al*., 2002; Liu et al., 2022). It comprises six formations, Dulahala Formation (H_1-H_3), Jianshan Formation (H_4-H_5), Halahuoqite Formation (H_6-H_8), Bilute Formation (H_9-H_{10}), Baiyinbaolage Formation (H_{11}-H_{12}), and Hujiertu

https://doi.org/10.1180/mgm.2024.90 Published online by Cambridge University Press

Formation (H_{13}-H_{18}) (Ling *et al*., 2012; Yang *et al*., 2017) (Fig.1).

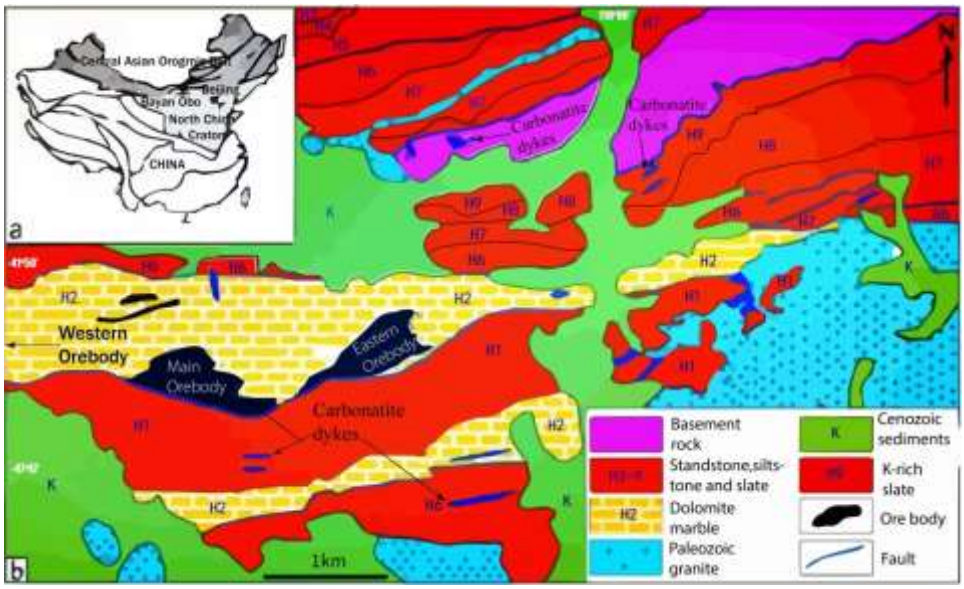

Figure 1. Geological sketch map of the Bayan Obo REE-Nb-Fe deposit (modified from Ling *et al*., 2013; Liu *et al*., 2022)

The specimens were picked up in magnetite ores within H8 formation in the eastern part of the mine (109°57.666′E, 41°47.951′N) (Fig.2). Parisite-(Nd) was associated with calcite, aegirine, magnetite, hematite, fluorite, riebeckite, bastnäsite-(Ce), barite, aeschynite-(Ce), aeschynite-(Nd), monazite, and parisite-(Ce). The ore-forming mechanism of Bayan Obo deposits is still controversial. There are many different viewpoints on mineralization age including (1) Mesoproterozoic to Neoproterozoic, 1360-789 Ma; (2) Caledonian, 485-386 Ma; (3) Hercynian, 277-255 Ma (Yuan, 2012; Xie *et al*., 2019). The models on the genesis of the Bayan Obo REE deposit include: (1) genetically related to carbonatite magmatism; (2) hydrothermal alteration of carbonate sedimentary rocks; (3) carbonatite volcanic eruptions and so on (Ren *et al*., 1994; Smith, 2007; Zhu *et al*., 2015; Yang *et al*., 2017). The formation of REE mineralized dolomite might be related to interaction and reaction between the carbonatite magmas and/or associated fluids with sedimentary carbonate rocks, with the REE-bearing carbonatite magmas having undergone intense fractionation enrichment process (Yang *et al*., 2024). Parisite-(Nd) might be a product of bimetasomatism Ca-Mg-carbonate rock and/or carbonatitie, and Na-, F-rich postmagmatic hydrothermal solutions.

https://doi.org/10.1180/mgm.2024.90 Published online by Cambridge University Press

Figure 2. The outcrop of specimen on which the new mineral parisite-(Nd) was found from main ore of Bayan Obo REE-Nb-Fe ore deposit

Appearance, physical and optical properties

Parisite-(Nd) occurs as subhedral to anhedral irregular grains from 0.02mm to 1mm in maximum dimension. The a:b:c ratio calculated from unit-cell parameters is 1: 0.5774: 2.3088. Parisite-(Nd) shows thin, tabular and hexagonal crystal habits, but most of the grains are broken and fractured. Parisite-(Nd) is transparent, yellowish-brown color (Fig.3), with pale yellow streak. It displays vitreous to resinous lustre. It has no fluorescence under shortwave (254nm) and longwave (366nm) ultraviolet radiation. The Mohs hardness is between 4 and 5, which is estimated from comparison with fluorite and parisite-(Ce). Cleavage is distinct on pseudo-{001} and parting was not observed. The fracture is uneven, or conchoidal, and the mineral tenacity is brittle. Density was not measured due to the limited crystals available and nanometric crystal size. The calculated density is 4.357 g/cm^3 on the basis of empirical formula and unit-cell volume from powder XRD data.

https://doi.org/10.1180/mgm.2024.90 Published online by Cambridge University Press

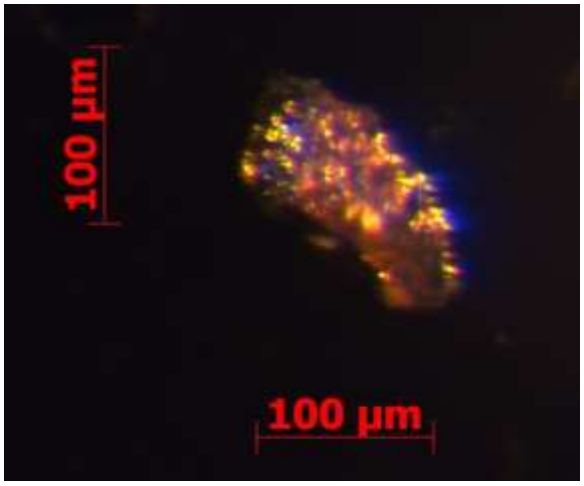

Figure 3. A microscopic view of yellowish-brown parisite-(Nd)

Under the polarizing microscope (Fig.4), parisite-(Nd) is colorless to brownish yellow in transmitted light with weak pleochroism. The other main optical characteristics of parisite-(Nd) are parallel extinction, interference color from third-order bluish yellow to fourth-order white, uniaxial and optically positive. In transmitted light parisite-(Nd) is colourless, pseudo-uniaxial (+), ω= (1.679), ε= (1.754) (the value not determined, data referenced from Zhang and Tao, 1986). The pleochroism is invisible.

https://doi.org/10.1180/mgm.2024.90 Published online by Cambridge University Press

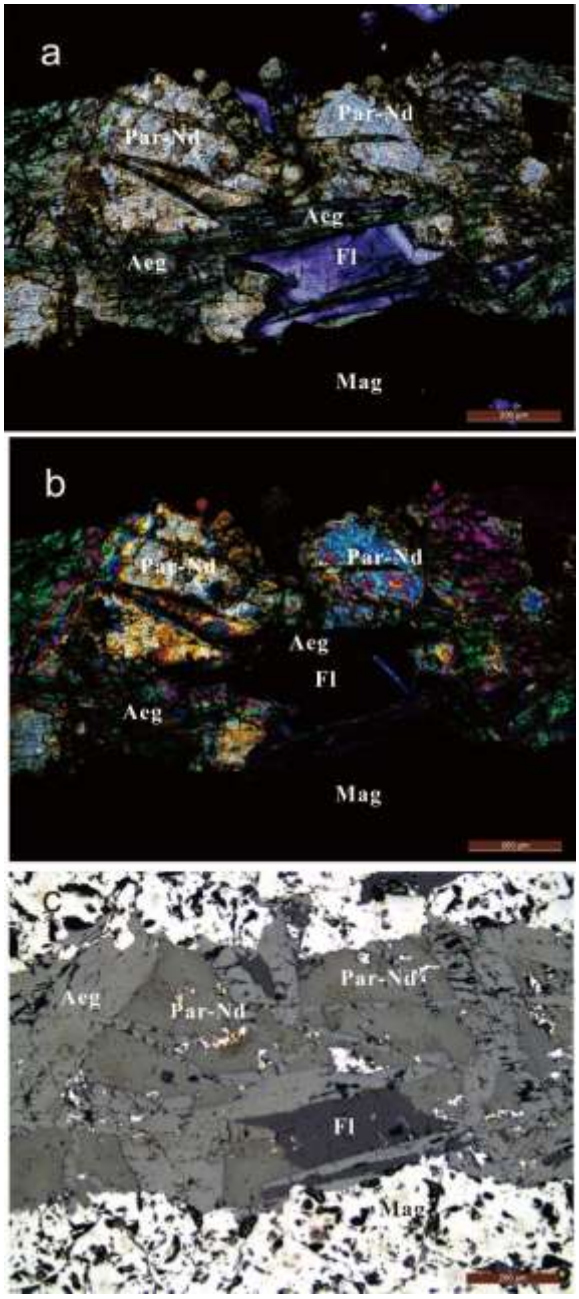

Figure 4. Photomicrographs of parisite-(Nd) (Par-Nd) associated with fluorite (Fl), aegirine (Aeg) and magnetite (Mag). (a) transmitted light; (b) cross polarized light; (c) reflected light

Raman Spectroscopic characterization

The Raman spectrum of parisite-(Nd) between 100 and 3600 cm^{-1} was recorded using a Renishaw inVia Reflex system, using a solid-state laser with a wavelength of 532 nm and a thermoelectric cooled CCD detector, with 1 cm^{-1} resolution and a spot size of 2 μm and compared with associated bastnäsite-(Ce) and parisite-(Ce) (Fig. 5).

https://doi.org/10.1180/mgm.2024.90 Published online by Cambridge University Press

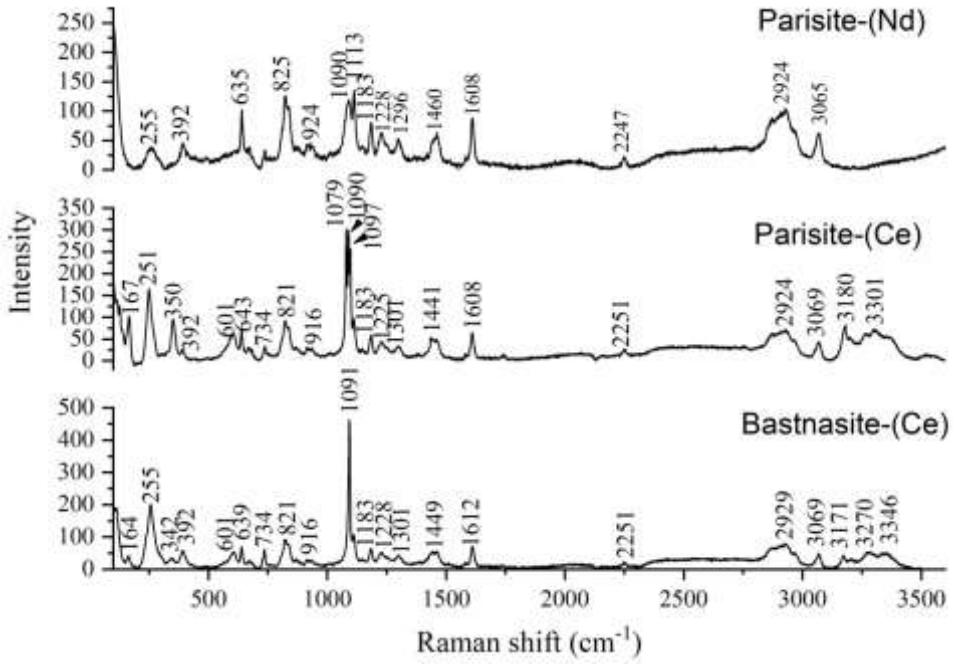

Figure 5. Raman spectra of parisite-(Nd) with comparison to parisite-(Ce) and bastnäsite-(Ce)

The strong and sharp peaks of parisite-(Nd) are observed at 1113, 1090, 825, 635 and 1608 cm-1 and moderate to weak bands centered at 255, 392, 739, 924, 1183, 1228, 1296, 1640, 2247, 2924 and 3065 cm^{-1}. The Raman spectrum of parisite-(Nd) is similar with the spectra of parisite-(Ce) and bastnäsite-(Ce), but the vibration of CO_3^{2-} show some different. The CO_3^{2-} complex exhibits four internal vibrational modes: (1) a symmetric stretching vibration (ν_1), (2) an out-of-plane bending vibration (ν_2), (3) a doubly degenerate asymmetric stretching vibration (ν_3) and (4) in-plane bending vibration (ν_4) (White, 1974). The most intense Raman band is assigned to ν_1 vibration at ~1100 cm^{-1}. The vibration spectrum of the $(CO_3)^{2-}$ in bastnäsite-(Ce) is relatively symmetrical, and the ν_1 Raman scattering peak is located at 1091cm^{-1}. The ν_1 Raman band is split into three bands at ~1079 cm^{-1}, ~1090 cm^{-1} and ~1097 cm^{-1} in parisite-(Ce), while two bands at ~1090 cm^{-1} and ~1113 cm^{-1} in parisite-(Nd). These differences of ν_1 Raman spectrum of fluorinated carbonates are probably dependent on the chemical compositions (Frost and Dickfos, 2007). The band assigned to the $\nu_2(CO_3)^{2-}$ vibration is supposed to locate at ~924 cm^{-1} and ~825cm^{-1} in parisite-(Nd), which is a little higher than the band positions at ~916 cm^{-1} and ~821 cm^{-1} in parisite-(Ce) and bastnäsite-(Ce). The parisite-(Nd) spectrum shows $\nu_3(CO_3)^{2-}$ vibration band at ca. 1460 cm^{-1} in comparison with 1441 cm^{-1} in parisite-(Ce) and 1449 cm^{-1} in bastnäsite-(Ce). The bands in the range of 600~740 cm^{-1} are supposed to be classified as the ν_4

https://doi.org/10.1180/mgm.2024.90 Published online by Cambridge University Press

bending mode. A sharp intensity band is observed at 635 cm^{-1} in parisite-(Nd), and two bands are observed at ~601 cm^{-1} and ~643 (639) cm^{-1} in parisite-(Ce) and bastnäsite-(Ce). A weaker peak at ~739 cm^{-1} or ~734 cm^{-1} is observed in three samples. The positions of the ν_4 bands perhaps show the divergence of ionic radius of the Nd and Ce cation in the carbonate structure. A number of low wavenumber bands are observed for parisite-(Nd) at ~392 cm^{-1} and ~255 cm^{-1}. These two bands and another two bands around 350 (342) cm^{-1} and 167 (164) cm^{-1} are also observed in the Raman spectra of parisite-(Ce) and bastnäsite-(Ce). These bands are described as lattice modes involving halogen and F (Frost and Dickfos, 2007). The Raman spectrum of all three flurocarbonate minerals in the 2800 to 3500 cm^{-1} spectral range is reported in Figure 5. Raman bands are observed at 2924 and 3065 cm^{-1}. These bands are attributed to water stretching vibrations (Frost *et al*., 2013). For parisite-(Nd) OH units are likely to replace F in a complex structure.

Chemical composition

The chemical composition of parisite-(Nd) was studied with a JXA-iHP200F electron microprobe, operating in wavelength-dispersive mode with excitation voltage of 15kV, specimen beam current 20nA, and 5 μm beam diameter. The analytical data of 13 spots with ranges and standards employed are given in Table 1. There is insufficient material for a direct determination of CO_2 and H_2O. Thus, the calculation of the empirical formula was done in following steps: (1) calculation of the REE site cations/Ca site cations ratio; (2) when REE site cations/Ca site cations =2, the normalization of the empirical formula to 3 cations (REE site cations + Ca site cations); (3) calculation of the OH content (in apfu) from charge balance considering 3 CO_3^{2-} groups and the calculated F content. The CO_2 was calculated to 24.44 wt% for charge neutrality. The empirical formula is $(Ca_{0.945}Fe_{0.058}Sr_{0.015}Ba_{0.007})_{\Sigma 1.025}(Nd_{0.967}Ce_{0.529}La_{0.191}Pr_{0.137}Gd_{0.070}Sm_{0.029}Th_{0.022}Y_{0.016}Nb_{0.011}Ho_{0.003})_{\Sigma 1.975}(CO_3)_3F_{1.893}OH_{0.023.}$ The simplified formula is $Ca(Nd,Ce,La,Pr,Gd)_2(CO_3)_3F_2$. The ideal formula is $CaNd_2(CO_3)_3F_2$, which requires (wt. %) CaO 10.26%, Nd_2O_3 61.56%, F 6.95%, CO_2 24.16%, O=F-2.93, total 100 wt.%. The ratio of rare earth to calcium is close to 2: 1. Neodymium plays an absolutely dominant role in rare earth elements, and this feature is different from parisite-(Ce) and parisite-(La).

https://doi.org/10.1180/mgm.2024.90 Published online by Cambridge University Press

Table 1. Chemical data (in wt %) for parisite-(Nd)

Constituent	Mean	Range	Stand. Dev. (σ)	Reference Material
F	6.60	5.26-7.70	0.60	topaz
La_2O_3	5.70	4.78-6.73	0.58	LaP_5O_{14}
Ce_2O_3	15.93	12.80-17.33	1.41	CeP_5O_{14}
Pr_2O_3	4.14	3.58-4.47	0.25	PrP_5O_{14}
Nd_2O_3	29.81	25.94-31.68	1.69	NdP_5O_{14}
Sm_2O_3	0.94	0.70-1.20	0.17	SmP_5O_{14}
Gd_2O_3	2.33	1.82-3.14	0.44	GdP_5O_{14}
Ho_2O_3	0.09	0-0.27	0.08	HoP_5O_{14}
Y_2O_3	0.33	0.11-0.51	0.13	YP_5O_{14}
CaO	9.71	8.45-10.67	0.64	wollastonite
FeO	0.77	0-2.41	0.59	fayalite
SrO	0.28	0.06-0.40	0.10	celestine
ThO_2	1.07	0.25-2.76	0.78	ThO_2
Nb_2O_5	0.28	0-1.12	0.30	$KNbO_3$
BaO	0.19	0-1.83	0.50	barite
H_2O*	0.21			
CO_2*	24.44			
-O=F	2.77			
Total	**100.05**			

* H_2O and CO_2 from formula calculation.

Crystallography

The crystal structure of parisite-(Nd) sample could not be determined by single-crystal X-ray studies due to the nature of nanometric crystals aggregate and its structural complexity. Therefore, the X-ray powder diffraction and selected-area electron diffraction were, instead, carried out for the crystallographic characterization.

X-ray powder diffraction data were collected with a Rigaku Xtalab Synergy single-crystal diffractometer (CuKα radiation) in Gandolfi powder mode at 50kV and 1mA. The unit-cell parameters were refined using the program by Holland and Redfern (1997). A monoclinic unit cell of parisite-(Ce) by Ni *et al* (2000) was referenced to index the diffraction spots. Unit cell parameters refined from the powder data are as follows: monoclinic symmetry with space group *Cc* (# 9), a = 12.3283(13), b = 7.1185(4) Å, c = 28.4633(37) Å, β = 98.529(14)°, V = 2470.28(42) $Å^3$, Z = 12.

The complete X-ray powder diffraction data of parisite-(Nd) is shown in Table 2 and compared with parisite-(Ce) and parisite-(La) in Figure 6. Based on the obtained XRD patterns of

https://doi.org/10.1180/mgm.2024.90 Published online by Cambridge University Press

parisite-(Nd), the results show that these values are in agreement with the measured *d*-spacings for parisite-(Ce), with most of the absolute value of difference less than 0.02 Å. The diagnostic reflexes with *d*-values (Å) of 14.336, 6.926, 4.720, 3.558, 2.835, 2.056, 1.959 and 1.880 for parisite are recognized. The interplanar spacings in *c* axis direction of parisite-(Nd) have some difference with those of parisite-(Ce) due to the substitution of Nd to Ce.

Table 2. X-ray powder diffraction data (d in Å, I in %) for parisite-(Nd)

h	*k*	*l*	I_{cal}	I_{meas}	d_{cal}	d_{meas}
0	**0**	**2**	**100.0**	**75**	**14.074**	**14.336**
0	**0**	**4**	**38.9**	**28**	**7.037**	**6.926**
0	**0**	**6**	**73.2**	**61**	**4.691**	**4.720**
$\bar{3}$	**1**	**1**	**78.1**	**80**	**3.559**	**3.558**
0	2	4	10.3	22	3.176	3.114
0	**2**	**6**	**53.4**	**100**	**2.836**	**2.835**
$\bar{3}$	**3**	**1**	**47.4**	**43**	**2.055**	**2.056**
0	**2**	**12**	**24.5**	**39**	**1.959**	**1.959**
3	**3**	**5**	**19.4**	**29**	**1.881**	**1.880**
0	4	0	9.9	14	1.780	1.777
6	2	4	12.0	20	1.662	1.663
3	3	11	8.1	10	1.544	1.542
6	2	10	6.1	8	1.415	1.415
$\bar{3}$	5	1	3.8	8	1.345	1.350
9	1	3	5.0	16	1.292	1.291
3	3	17	3.5	12	1.243	1.245

https://doi.org/10.1180/mgm.2024.90 Published online by Cambridge University Press

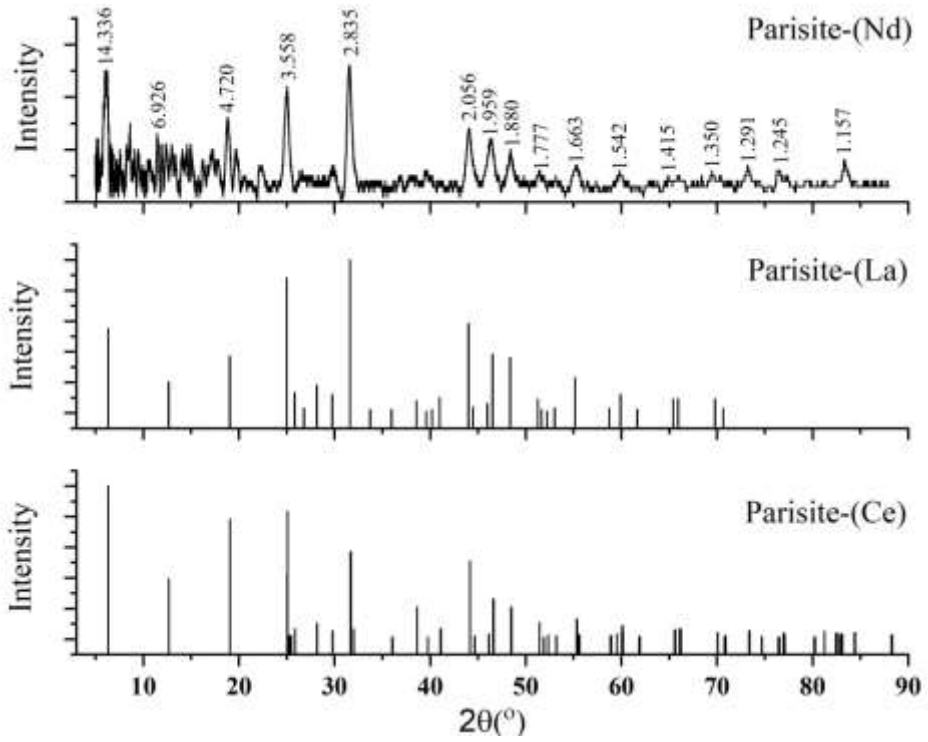

Figure 6. Powder X-ray diffraction patterns of parisite-(Nd) in this work with comparison to parisite-(Ce) (Ni *et al*., 2000) and parisite-(La) (Menezes Filho *et al*., 2018)

For TEM studies, two perpendicular TEM foils of about 80nm thickness were prepared with a FEI Scois 2 focus ion beam (FIB) device at Beijing SHRIMP Center, Institute of Geology, Chinese Academy of Geological Sciences, and analyzed by a JEM–2100 (HR) Transmission Electron Microscope equipped with a double–tilt holder, a Gatan digital camera, and an INCA Energy TEM100 energy–dispersive spectroscopy instrument at the Institute of Mineral Resources, Chinese Academy of Geological Sciences, operated at 200 kV. Images of one foil and its location in polished section before cutting are shown in Figure 7. Before TEM testing on parisite-(Nd), the TEM instrument underwent camera constant calibration using a standard polycrystalline gold sample. Following calibration, the camera constant was determined to be $L\lambda = 9.26$ mm·Å. Six different SAED patterns were acquired along two distinct Kikuchi lines within the same area of one TEM foil and simulated in Kikuchi maps using SingleCrystal program (Figure 8 and 9), while three different SAED patterns (Figure 10) were captured along a Kikuchi line in another TEM foil.

https://doi.org/10.1180/mgm.2024.90 Published online by Cambridge University Press

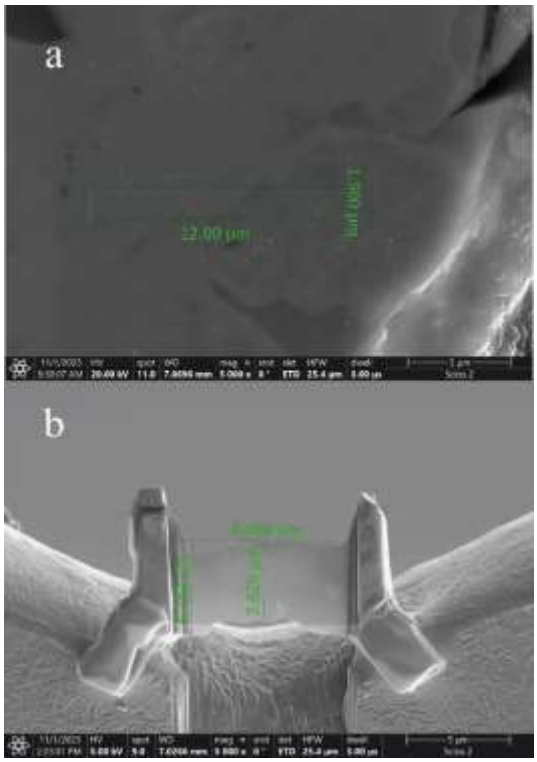

Figure 7. Images of TEM foil of parisite-(Nd) by FIB sampling for SAED analysis

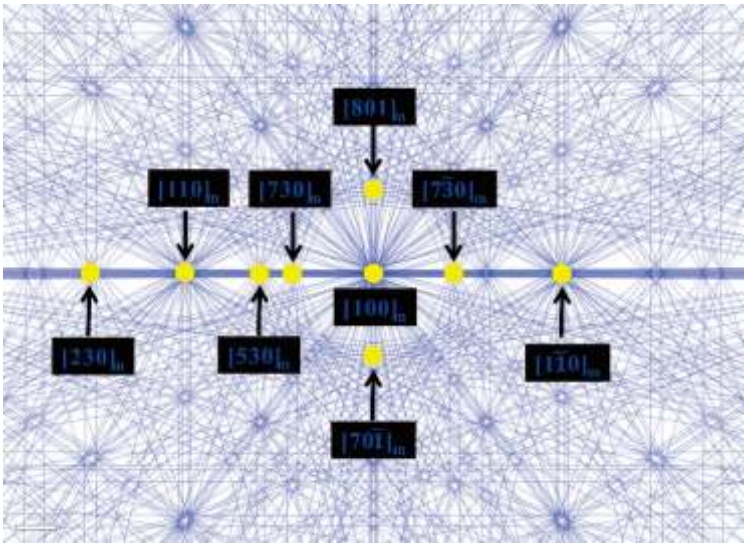

Figure 8. Kikuchi map of parisite-(Nd) simulated using SingleCrystal software (Palmer, 2015). The labeled Kikuchi poles in the diagram correspond to the zone axes of SAED patterns in Figure 9

The solid angles calculated from the patterns match with the patterns generated from the structure of parisite-(Ce) (Fig.9). A series of SAED patterns were taken along two kikuchi lines. Figure 9 shows the SAED patterns and the indices of the diffraction spots of zones [100], [7$\bar{3}$0], [1$\bar{1}$0], [730], [801] and [70$\bar{1}$], which conform to the monoclinic symmetry of parisite-(Ce). Figure

https://doi.org/10.1180/mgm.2024.90 Published online by Cambridge University Press

10 shows the SAED patterns of the diffraction spots of zones [001], [809] and [403]. We also measured the angles between adjacent planes in the SAED patterns of parisite-(Nd). The measured angles of parisite-(Nd) agree well with the calculated angles of parisite-(Ce), with the absolute value of difference less than 1° (Table 3).

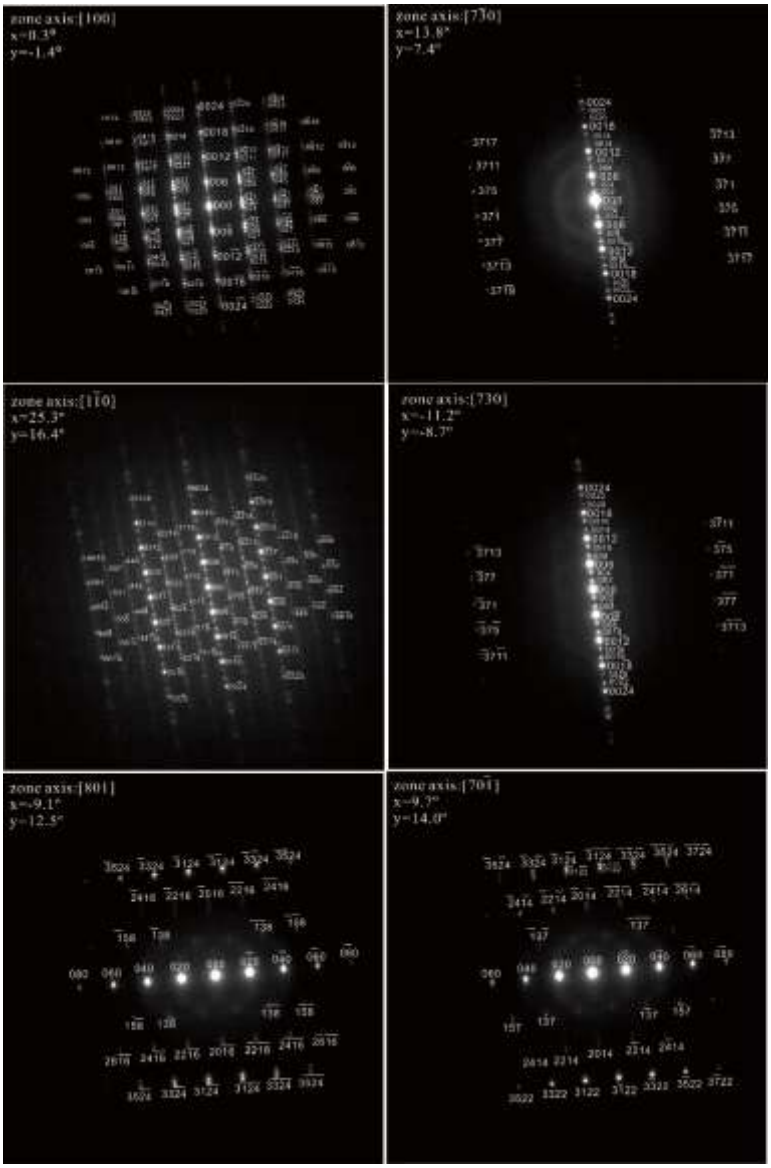

Figure 9. SAED patterns of parisite-(Nd) from 6 different zone axes around [001] axis with the diffraction spots of zones [100], [7$\bar{3}$0], [1$\bar{1}$0], [730], [801] and [70$\bar{1}$]

Table 3. Measured angles of parisite-(Nd) in comparison with calculated angles of parisite-(Ce)

Planes	Angle between planes	
(*hkl*)	Measured	Calculated
(006)/(0$\bar{2}$0)	90	90
(006)/(0$\bar{2}$6)	53.24	52.67
(0$\bar{2}$0)/(0$\bar{2}$6)	36.94	37.33

https://doi.org/10.1180/mgm.2024.90 Published online by Cambridge University Press

(006)/(37$\bar{1}$)	89.56	90.03
(006)/(375)	77.89	78.08
(37$\bar{1}$)/(375)	11.67	11.94
(006)/($\bar{1}\bar{1}$3)	60.66	59.55
(006)/($\bar{1}\bar{1}$9)	28.59	27.65
(006)/($\bar{3}\bar{3}$1)	90.55	89.95
(006)/($\bar{3}\bar{3}$7)	67.12	66.20
(00$\bar{6}$)/($\bar{3}$71)	90.44	90.03
(00$\bar{6}$)/($\bar{3}$7$\bar{5}$)	78.65	78.08
(020)/($\bar{3}\bar{1}$24)	99.07	99.31
(020)/ ($\bar{3}$124)	80.87	80.69
(020)/($\bar{3}\bar{1}\bar{2}\bar{2}$)	99.50	99.32
(020)/($\bar{3}\bar{1}\bar{2}\bar{2}$)	80.51	80.68

Measured = measured values based on the SAED patterns of parisite-(Nd) in Figure 9, Calculated = calculated values based on the cell parameters of parisite-(Ce) (Ni *et al*., 2000)

Parisite-(Nd) is the Nd-dominant analogue of parisite-(Ce), as demonstrated by the consistency between their chemical compositions, powder X-ray diffraction data and TEM results. The ionic radius of Nd^{3+} is 0.983 Å, which is close to the ionic radius of Ce^{3+}(1.01 Å), and La^{3+} (1.032 Å) (Shannon 1976). The rare elements occupy the same position in the parisite crystal structure. So parisite-(Nd) is believed to have the same structure as parisite-(Ce) (Ni *et al*., 2000).

https://doi.org/10.1180/mgm.2024.90 Published online by Cambridge University Press

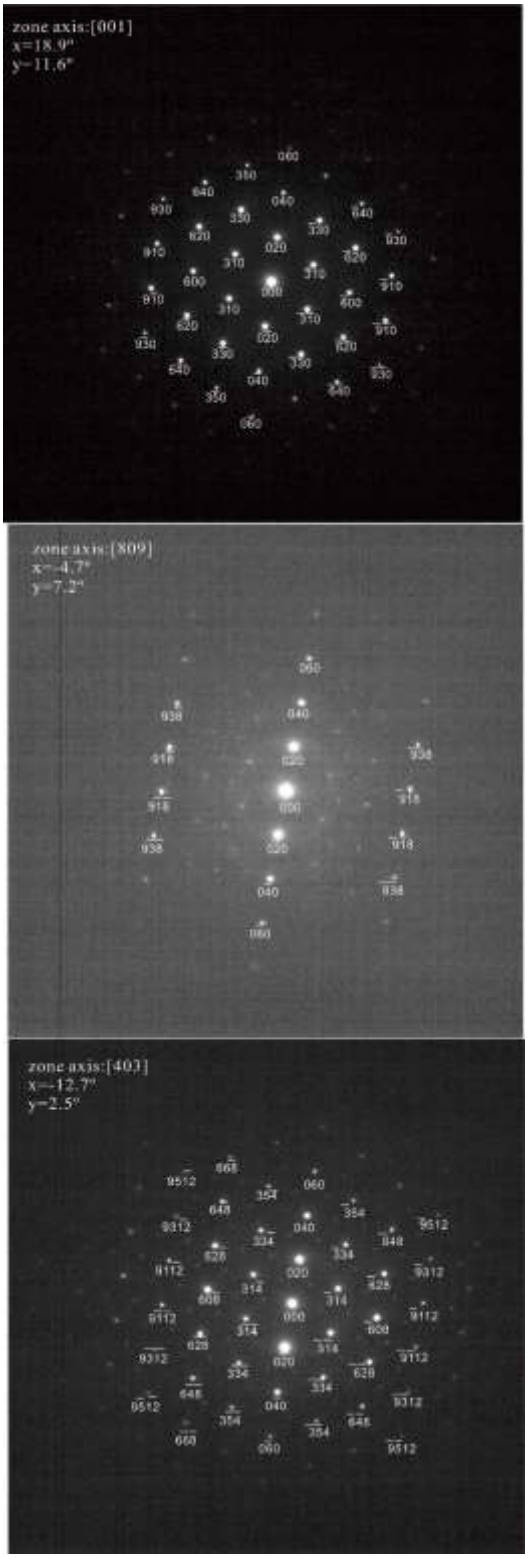

Figure 10. SAED patterns of parisite-(Nd) of the diffraction spots of zones [001], [809] and [403]

https://doi.org/10.1180/mgm.2024.90 Published online by Cambridge University Press

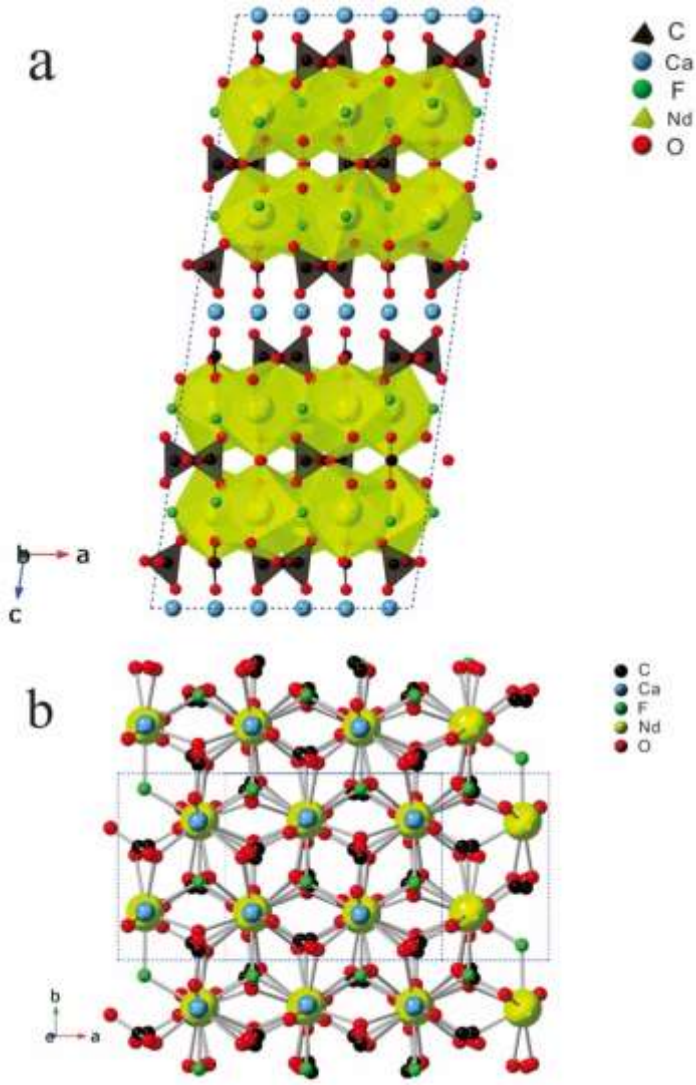

Figure 11. The crystal structure of parisite-(Nd) modified from parisite-(Ce) by Ni *et al* (2000) using CrystalMaker software (Palmer, 2015)

Discussion

As a member of Ca-REE flurocarbonate minerals, minerals chemically or structurally related to parisite-(Nd) including bastnäsite, synchysite, and röntgenite are shown in Table 4 and Table S1. The structure of Ca-REE flurocarbonate family of minerals has been described quantitatively in terms of layers parallel to (001) of the hexagonal or monoclinic cell. There are some ways to describe the structure of Ca-REE flurocarbonate family of minerals. The mostly used notation is proposed to use two end members bastnäsite (*B*) and synchysite (*S*) for the characterization of layer sequences in fluorcarbonate minerals (Van Landuyt and Amelinckx, 1975; Meng *et al*., 2001a; Meng *et al*., 2001b). Another way for the interpretation of the stacking sequence can be

https://doi.org/10.1180/mgm.2024.90 Published online by Cambridge University Press

defined in terms of vaterite (V) and bastnäsite (B) (Ciobanu et al., 2017; Capitani et al., 2019; Capitani et al., 2020). The structure can also be described in terms of four layers parallel to (001): a REEF structural layer (*d*), a layer of CO_3 groups between two REEF layers (*e*), a layer of Ca (*f*), and a layer of CO_3 groups between calcium and REEF layers (*g*) (Donnay and Donnay, 1953).

The structure of parisite-(Nd) is regarded as the intermediate product composed of 1:1 ratio of B and S or 2:1 ratio of B and V or *dedgfg* structure along the (00l) plane (Figure 11a) (Donnay and Donnay, 1953). Referring to the structure of parisite-(Ce), Nd atoms coordinate to three F atoms in the same (001) layer and six O atoms, three from the neighboring (CO_3) groups on each side. Ca atoms coordinate with eight O atoms, four from each adjoining (CO_3) layer; the six shorter Ca-O bonds form a regular octahedron (Figure 11b). The parisite-(Nd) structure consists of stacked (001) layers of the Nd polyhedra and Ca polyhedra. The polyhedra within the layers share edges, and the polyhedra between the layers are connected by apical oxygen atoms and by vertically oriented carbonate groups (Ni *et al*., 2000).

Not only the nature of the nanometric crystals aggregate of the parisite-(Nd) sample, but also structural complexity makes its crystal structure very difficult to determine. Because the X-ray diffraction power of F, O and C atoms is very weak, it is difficult to calculate the structure factor. In addition, a variety of syntactic intergrowth, polytypes, polysomatic faults, polytypic disorder and twinning have been also found in parisite-(Ce) as well as in parisite-(Nd) in our observation, which brought great difficulties in analysis of X-ray studies (Wu and Meng, 2000; Meng *et al*., 2001a, 2001b; Ciobanu *et al*., 2017; Capitani, 2019). Taking parisite-(Ce) as an example, its structure was defined with space group *R*3, *a*=7.18 Å, *c*=8.41 Å in the early study (Donnay and Donnay, 1953). Until the work of Ni *et a*l (2000), the crystal structure of parisite-(Ce) was refined to space group *C*2/*c* or *Cc* with unit cell of a = 12.305(2), b = 7.1053(5), c = 28.250(5) Å, and β = 98.257(14)°. In this study, it was proposed for the first time that the common 6R polytype of parisite was not found, and it may be 2M polytype. Capitani *et al* (2019) proposed the discovery of a new polytype with C1 space group may be $2M_2$, and believed that rhombohedral symmetry in parisite was wrong. The structure of parisite-(La) proved the result of simulation calculation with Ni *et al* (2000)'s work. However, due to inclusions of synchysite, röntgenite or bastnäsite microblocks, no new structure was determined for parisite-(La) (Hålenius *et al*., 2016; Menezes Filho *et al*., 2018). In our study, we tried to analyse several particles of parisite-(Nd) many times

https://doi.org/10.1180/mgm.2024.90 Published online by Cambridge University Press

on a Rigaku Xtalab Synergy-DS 4-circle diffractometer with CuKα radiation but failed. The X-ray powder diffraction and selected-area electron diffraction were, instead, carried out for the crystallographic characterization to prove the structure of parisite-(Nd) analogue of parisite-(Ce).

Table 4. Minerals and phases chemically/structurally related to parisite-(Nd)

Mineral	Formula	Crystal system	Space group	Cell parameters					Reference
				a (Å)	*b* (Å)	*c* (Å)	*β* (°)	Z	
Parisite-(Nd)	$CaNd_2(CO_3)_3F_2$	Monoclinic	*Cc*	12.3283	7.1185	28.4633	98.529	12	This study
Parisite-(Ce)	$Ca(Ce,La)_2(CO_3)_3F_2$	Monoclinic	*Cc*	12.3049	7.1056	28.2478	98.2416	12	Donnay and Donnay, 1953 Ni *et al.*, 2000
Parisite-(La)	$CaLa_2(CO_3)_3F_2$	Monoclinic	*C*2, *Cm* or *C*2/*m*	12.356	7.1368	28.299	98.342	12	Menezes Filho *et al.*, 2018
Synchysite-(Ce)	$Ca(Ce,La)(CO_3)_2F$	Monoclinic	*C*2/*c*	12.329	7.110	18.741	102.68	12	Wang *et al.*, 1994
Synchysite-(Nd)	$Ca(Nd,La)(CO_3)_2F$	Orthorhombic		4.039	6.984	54.27		12	Scharm and Kühn, 1983
Synchysite-(Y)	$Ca(Y,Ce)(CO_3)_2F$	Monoclinic	*C*2/*c*	12.039	6.950	18.436	102.45	12	Smith *et al.*, 1960
Röntgenite-(Ce)	$Ca_2(Ce,La)_3(CO_3)_5F_3$	Trigonal	*R*3	7.13		69.4		9	Donnay and Donnay, 1953
Bastnäsite-(Ce)	$(Ce,La)(CO_3)F$	Hexagonal	$P\bar{6}2c$	7.118		9.762		6	Palache *et al.*, 1951

https://doi.org/10.1180/mgm.2024.90 Published online by Cambridge University Press

Bastnäsite-(La)	(La, Ce)(CO_3)F	Hexagonal	$P\bar{6}2c$				Ni *et al.*, 1993 Vainshtein *et al.*, 1961
Bastnäsite-(Nd)	Nd(CO_3)F	Hexagonal	$P\bar{6}2c$	7.0792	9.721	6	Miyawaki *et al.*, 2013
Bastnäsite-(Y)	Y(CO_3)F	Hexagonal	$P\bar{6}2c$	6.57	9.48	6	Mineev *et al.*, 1970

Acknowledgements

This research is funded by Fundamental Research Project of Chinese Academy of Geological Sciences (JKYZD202324) and China Geological Survey Project (DD20242852). We acknowledge all members of the IMA Commission on New Minerals, Nomenclature and Classification, Professor Ferdinando Bosi, and three anonymous reviewers for their helpful suggestions and comments. Dr Li Ting and Dr Chen Zhi are greatly acknowledged for the help of single X-ray diffraction analysis.

References

Bosi, F., Hatert, F., Pasero, M., and Mills, S. J. (2024). IMA Commission on New Minerals, Nomenclature and Classification (CNMNC)–Newsletter 80. *European Journal of Mineralogy*, **36**, 599-604.

Capitani, G. (2019). HRTEM investigation of bastnäsite–parisite intergrowths from Mount Malosa (Malawi): Ordered sequences, polysomatic faults, polytypic disorder, and a new parisite-(Ce) polymorph. *European Journal of Mineralogy*, **31**, 429-442.

Capitani, G. (2020). Synchysite-(Ce) from Cinquevalli (Trento, Italy): stacking disorder and the polytypism of (Ca, REE)-fluorcarbonates. *Minerals*, **10**, 77.

Castor, S. B. (2008). The Mountain Pass rare-earth carbonatite and associated ultrapotassic rocks, California. *The Canadian Mineralogist*, **46(4)**, 779-806.

https://doi.org/10.1180/mgm.2024.90 Published online by Cambridge University Press

Ciobanu, C. L., Kontonikas-Charos, A., Slattery, A., Cook, N. J., Ehrig, K. and Wade, B. P. (2017). Short-range stacking disorder in mixed-layer compounds: A HAADF STEM study of bastnäsite-parisite intergrowths. *Minerals*, **7**, 227.

Donnay, G. and Donnay, J.D.H. (1953). The crystallography of bastnäsite, parisite, roentgenite, and synchisite. *American Mineralogist: Journal of Earth and Planetary Materials*, **38**, 932-963.

Doroshkevich, A. G., Viladkar, S. G., Ripp, G. S., and Burtseva, M. V. (2009). Hydrothermal REE mineralization in the Amba Dongar carbonatite complex, Gujarat, India. *The Canadian Mineralogist*, **47(5)**, 1105-1116.

Frost, R. L. and Dickfos, M. J. (2007). Raman spectroscopy of halogen-containing carbonates. *Journal of Raman Spectroscopy: An International Journal for Original Work in all Aspects of Raman Spectroscopy, Including Higher Order Processes, and also Brillouin and Rayleigh Scattering*, **38**, 1516-1522.

Frost, R.L., López, A., Scholz, R., Xi, Y. and Belotti, F.M. (2013) Infrared and Raman spectroscopic characterization of the carbonate mineral huanghoite – and in comparison with selected rare earth carbonates. *Journal of Molecular Structure*, **1051**, 221-225.

Guastoni, A., Kondo, D., and Nestola, F. (2010). Bastnäsite-(Ce) and Parisite-(Ce) From Mt. Malosa, Malawi. *Gems & Gemology*, **46(1)**,42-47.

Hålenius, U., Hatert, F., Pasero, M. and Mills, S.J. (2016). New minerals and nomenclature modifications approved in 2016. Newletter 32. IMA No. 2016-031. *Minerlogical Magazine*, **80(5)**, 920-921.

Holland, T.J.B. and Redfern, S.A.T. (1997) Unit cell refinement from powder diffraction data: the use of regression diagnostics. *Mineralogical Magazine*, **61**, 65-77.

Jambor, J.L., Burke, E.A., Ercit, T.S. and Grice, J.D.(1988) New mineral names. *American Mineralogist*, **73**, 1496-1497.

Ling, M. X., Liu, Y. L., Williams, I. S., Teng, F. Z., Yang, X. Y., Ding, X., Wei, G.J., Xie, L.H., Deng, W.F., and Sun, W. D. (2013). Formation of the world's largest REE deposit through protracted fluxing of carbonatite by subduction-derived fluids. *Scientific reports*, **3(1)**, 1776.

Liu, T., Song, W., Kynicky, J., Yang, J., Chen, Q., and Tang, H. (2022). Automated quantitative characterization REE ore mineralogy from the giant Bayan Obo Deposit, Inner Mongolia, China. *Minerals*, **12(4)**, 426.

Menezes Filho, L. A., Chaves, M. L., Chukanov, N. V., Atencio, D., Scholz, R., Pekov, I., da Costa, G.M., Morrison, S.M., Andrade, M.B., Freitas, E.T.F., Downs, R.T. and Belakovskiy, D. I. (2018). Parisite-(La), ideally $CaLa_2(CO_3)_3F_2$, a new mineral from Novo Horizonte, Bahia, Brazil. Mineralogical Magazine, 82, 133-144.

Meng, D., Wu, X., Mou, T. and Li, D. (2001a). Determination of six new polytypes in parisite-(Ce) by means of high resolution electron microscopy. *Mineralogical Magazine*, **65**, 797-806.

Meng, D., Wu, X., Mou, T. and Li, D. (2001b). Microstructural investigation of new polytypes of parisite-(Ce) by high-resolution transmission electron microscopy. *The Canadian Mineralogis*t, **39**, 1713-1724.

Mineev, D.A., Lavrischeva, T.I. and Bykova, A.V. (1970). Yttrian bastnaesite-an alteration product of gagarinite. *Zapiski Vsesoyuznogo Mineralogicheskogo Obshchestva*, **99**, 328-332.

Miyawaki, R., Yokoyama, K. and Husdal, T. A.(2013). Bastnäsite-(Nd), a new Nd-domninant member of the bastnäsite group from the Stetind pegmatite, Tysfjord, Nordland, Norway. *European Journal of Mineralogy*, **25**, 187-191.

Morteani, G. (1991). The rare earths; their minerals, production and technical use. *European Journal of mineralogy*, **3(4)**, 641-650.

Ni, Y., Hughes, J.M. and Mariano, A.N. (1993). The atomic arrangement of bastnäsite-(Ce), $Ce(CO_3)F$, and structural elements of synchysite-(Ce), röntgenite-(Ce), and parisite-(Ce). *American Mineralogist*, **78**, 415-418.

Ni, Y., Post, J. E. and Hughes, J.M. (2000) The crystal structure of parisite-(Ce), $Ce_2CaF_2(CO_3)_3$. *American Mineralogist*, **85**, 251-258.

Nie, F. J., Jiang, S. H., Su, X. X., and Wang, X. L. (2002). Geological features and origin of gold deposits occurring in the Baotou–Bayan Obo district, south-central Inner Mongolia, People's Republic of China. *Ore Geology Reviews*, **20(3-4)**, 139-169.

Oftedal, I.(1931) Zur kristallstruktur von bastnasit (Ce,La-)FCO_3. *Zeitschrift fur Kristallographie*, **78**, 462-469.

https://doi.org/10.1180/mgm.2024.90 Published online by Cambridge University Press

Palache, C., Berman, H. and Frondel, C. (1951) Dana's system of mineralogy, (7th edition), v. II, 289-291.

Palmer, D. C. (2015). Visualization and analysis of crystal structures using CrystalMaker software. *Zeitschrift für Kristallographie – Crystalline Materials*, **230**(9-10), 559-572.

Ren, Y., Zhang, Y., Zhang, Z. (1994). Study on heat events of ore forming in the Bayan Obo deposit. *Acta Geoscience Sinica*, **30**, 95-101(in Chinese with English abstract)

Scharm, B. and Kühn, P. (1983). Synchysite-(Nd), Ca (Nd,Y,Gd), a new mineral. *Neues Jahrbuch für Mineralogie, Monatshefte*, 201.

Seifert, W., Kämpf, H., and Wasternack, J. (2000). Compositional variation in apatite, phlogopite and other accessory minerals of the ultramafic Delitzsch complex, Germany: implication for cooling history of carbonatites. *Lithos*, **53(2)**, 81-100.

Smith, W.L., Stone, J., Ross, D.R. and Levine, H.(1960). Doverite [= synchysite-(Y)], a possible new yttrium fluocarbonate from Dover, Morris Co., New Jersey. *American Mineralogist*, **45**, 92-98.

Smith, M. P. (2007). Metasomatic silicate chemistry at the Bayan Obo Fe–REE–Nb deposit, Inner Mongolia, China: contrasting chemistry and evolution of fenitising and mineralising fluids. *Lithos*, **93(1-2)**, 126-148.

Vainshtein, E.E., Pozharitskaya, L.K. and Turanskaya, N.V. (1961). Behavior of rare earths in the process of carbonatite formation. *Geokhimiya*, **11**, 1031–1034 (in Russian).

Van Landuyt, J., and Amelinckx, S. (1975). Multiple beam direct lattice imaging of new mixed-layer compounds of the bastnaesite-synchisite series. *American Mineralogist: Journal of Earth and Planetary Materials*, **60**, 351-358.

Wang, L., Ni, Y. and Hughes, J.M. (1994). The atomic arrangement of synchysite-(Ce), $CeCaF(CO_3)_2$. *The Canadian Mineralogist*, **32**, 865-871.

Warren, C. H., and Palache, C. (1911, July). The pegmatites of the riebeckite-aegirite granite of Quincy, Mass., USA; their structure, minerals, and origin. In Proceedings of the American Academy of Arts and Sciences (Vol. 47, No. 4, pp. 125-168). American Academy of Arts & Sciences.

White, W.B. (1974). The carbonate minerals. In: Farmer VC (ed) The infrared spectra of minerals, Mineral Soc Monogr, vol 4. Mineral Soc, London, pp 227-284.

https://doi.org/10.1180/mgm.2024.90 Published online by Cambridge University Press

Wu, X., Meng, D., Pan, Z., Yang, G., and Li, D. (1998). Transmission electron microscopic study of new, regular, mixed-layer structures in calcium-rare-earth fluorocarbonate minerals. *Mineralogical Magazine*, **62(1)**, 55-64.

Wu, X.L. and Meng, D.W. (2000). Study on microstructure and ultrastructure of calcium-cerium fluoride carbonate minerals by transmission electron microscopy. China University of Geosciences Press, Wuhan. (in Chinese).

Xie, Y.L., Qu, Y.W., Yang, Z. F., Liang, P., Zhong, R.C., Wang, Q.W., Xia, J.M. and Li, B.C. (2019) Giant Bayan Obo Fe-Nb-REE deposit: progresses, controversaries and new understandings. *Mineral Deposits*, **38**, 983-1003 (in Chinese).

Yang, X., Lai, X., Pirajno, F., Liu, Y., Mingxing, L., and Sun, W. (2017). Genesis of the Bayan Obo Fe-REE-Nb formation in Inner Mongolia, north China craton: a perspective review. *Precambrian Research*, **288**, 39-71.

Yang, J., Song, W., Liu, Y., Zhu, X., Kynicky, J. and Chen, Q. (2024). Mineralogy and element geochemistry of the Bayan Obo (China) carbonatite dykes: Implications for REE mineralization. *Ore Geology Reviews*, 105873.

Yuan, Z.X. (2012). Discussion on the metallogenic age and genesis of Bayan Obo deposit. *Acta Geologica Sinica*, **86**, 683-686 (in Chinese).

Zeug, M., Nasdala, L., Ende, M., Habler, G., Hauzenberger, C., Chanmuang N, C., Škoda, R., Topa, D., Wildner, M. and Wirth, R. (2021). The parisite-(Ce) enigma: challenges in the identification of fluorcarbonate minerals. *Mineralogy and Petrology*, **115**,1-19.

Zhang, P.S. and Tao, K.J.(1986). Bayan Obo mineralogy. Science Publisher, Beijing, China. 208 p. (in Chinese with English summary).

Zhu, X. K., Sun, J., and Pan, C. (2015). Sm-Nd isotopic constraints on rare-earth mineralization in the Bayan Obo ore deposit, Inner Mongolia, China. *Ore Geology Reviews*, 64, 543-553

Figure captions

Figure 1. Geological sketch map of the Bayan Obo REE-Nb-Fe deposit (modified from Ling *et al*., 2013; Liu *et al*., 2022)

Figure 2. The outcrop of specimen on which the new mineral parisite-(Nd) was found from main ore of Bayan Obo REE-Nb-Fe ore deposit

Figure 3. A microscopic view of yellowish-brown parisite-(Nd)

Figure 4. Photomicrographs of parisite-(Nd) (Par-Nd) associated with fluorite (Fl), aegirine (Aeg) and magnetite (Mag). (a) transmitted light; (b) cross polarized light; (c) reflected light

Figure 5. Raman spectra of parisite-(Nd) with comparison to parisite-(Ce) and bastnäsite

Figure 6. Powder X-ray diffraction patterns of parisite-(Nd) in this work with comparison to parisite-(Ce) (Ni *et al*., 2000) and parisite-(La) (Menezes Filho *et al*., 2018)

Figure 7. Images of TEM foil of parisite-(Nd) by FIB sampling for SAED analysis

Figure 8. Kikuchi map of parisite-(Nd) simulated using SingleCrystal software (Palmer, 2015). The labeled Kikuchi poles in the diagram correspond to the zone axes of SAED patterns in Figure 9.

Figure 9. SAED patterns of parisite-(Nd) from 6 different zone axes around [001] axis with the diffraction spots of zones [100], [$7\bar{3}0$], [$1\bar{1}0$], [730], [801] and [$70\bar{1}$]

Figure 10. SAED patterns of parisite-(Nd) of the diffraction spots of zones [001], [809] and

https://doi.org/10.1180/mgm.2024.90 Published online by Cambridge University Press

[403]

Figure 11. The crystal structure of parisite-(Nd) modified from parisite-(Ce) by Ni *et al* (2000) using CrystalMaker software (Palmer, 2015)

https://doi.org/10.1180/mgm.2024.90 Published online by Cambridge University Press